Phage capsid nanoparticles with defined ligand arrangement block influenza virus entry - An antiviral strategy

Daniel Lauster[1 +], Simon Klenk[2,12 +], Kai Ludwig[3], Saba Nojoumi[4], Sandra Behren[2,12], Lutz Adam[2,12], Marlena Stadtmüller[5], Sandra Saenger[5], Stephanie Franz[5], Katja Hönzke[6], Ling Yao[6], Ute Hoffmann[7], Markus Bardua[7], Alf Hamann[7], Martin Witzenrath[6], Leif E. Sander[6], Thorsten Wolff[5], Andreas C. Hocke[6], Stefan Hippenstiel[6], Sacha De Carlo[8], Jens Neudecker[9], Klaus Osterrieder[10], Nediljko Budisa[4], Roland R. Netz[11], Christoph Böttcher[3], Susanne Liese[11]*, Andreas Herrmann[1]*, Christian P. R. Hackenberger[2,12]*

Affiliations:

[1]Institut für Biologie, Molekulare Biophysik, IRI Life Sciences, Humboldt-Universität zu Berlin, Invalidenstr. 42, 10115 Berlin, Germany.

[2]Leibniz-Forschungsinstitut für Molekulare Pharmakologie (FMP), Robert-Rössle-Str. 10, 13125 Berlin, Germany.

[3]Forschungszentrum für Elektronenmikroskopie und Gerätezentrum BioSupraMol, Institut für Chemie und Biochemie, Freie Universität Berlin, Fabeckstr. 36a, 14195 Berlin, Germany.

[4]Institut für Chemie, Biokatalyse, Technische Universität Berlin, Müller-Breslau-Straße 10, 10623 Berlin, Germany, and Department of Chemistry, University of Manitoba, Dysart Rd. 144, R3T 2N2, Winnipeg, Canada.

[5]Robert Koch Institut, FG 17 Influenzaviren und weitere Viren des Respirationstraktes, 13353 Berlin, Germany.

[6]Medizinische Klinik mit Schwerpunkt Infektiologie und Pneumologie, Charité – Universitätsmedizin Berlin, Partner von Freie Universität Berlin, Humboldt-Universität zu Berlin und Berlin Institute of Health, 10117 Berlin, Virchowweg 9, Germany.

[7]Experimentelle Rheumatologie, Deutsches Rheuma-Forschungszentrum Berlin, ein Leibniz-Institut, Charitéplatz 1, 10117 Berlin, Germany.

[8]Thermo Fisher Scientific, Achtseweg Noord 5, 5651 GG Eindhoven, The Netherlands.

[9]Chirurgische Klinik, Campus Mitte/Campus Virchow Klinikum, Charité – Universitätsmedizin Berlin, Partner von Freie Universität Berlin, Humboldt-Universität zu Berlin, und Berlin Institute of Health, 13353 Berlin, Augustenburger Platz 1, Germany

[10] Institut für Virologie, Robert von Ostertag-Haus, Zentrum für Infektionsmedizin, Freie Universität Berlin, 14163, Berlin Robert Von Ostertag-Str. 7 – 13, Germany.

[11]Fachbereich Physik, Theoretische Biophysik und Physik weicher Materie, Freie Universität Berlin, Arnimallee 14, 14195 Berlin, Germany. Currently: Department of Mathematics, University of Oslo (UiO), P.O. Box 1053, Blindern, NO-0316 Oslo, Norway

[12]Institut für Chemie, Humboldt-Universität zu Berlin, Brook-Taylor-Straße 2, 12489 Berlin, Germany.

*Correspondence to: susanlie@math.uio.no, andreas.herrmann@rz.hu-berlin.de, hackenbe@fmp-berlin.de

[+]Equal contribution

Introductory Paragraph:

Multivalent interactions at biological interfaces occur frequently in nature and mediate recognition and interactions in essential physiological processes such as cell-to-cell adhesion. Multivalency is one principle that allows a tight binding between pathogens and host cells during the initial stages of infection. One promising, yet challenging, approach to prevent infection is the design of synthetic or semisynthetic multivalent binders that interfere with pathogen adhesion[1-4].

We present a new approach for such a multivalent binder that is based on a spatially defined arrangement of ligands for influenza A virus. Complementary experimental and theoretical approaches demonstrate that bacteriophage capsids, which carry host cell virus ligands in an arrangement matching the geometry of binding sites of a viral spike protein, can bind to viruses in a defined multivalent mode. As visualized by cryo-electron tomography, these capsids cover the entire target, thus preventing its binding to the host cell. As a consequence, infection by influenza viruses is inhibited *in vitro, ex vivo* and *in vivo*. We conclude that, highly functionalized capsids present an alternative to strategies that target virus entry by spike-inhibiting antibodies[5] and peptides[6] or address late steps of the viral replication cycle[7].

Main Text:

Viral spike proteins such as those expressed by influenza A virus (IAV) are illuminating examples of how multivalent interactions contribute to infection processes. Hemagglutinin (HA), the major spike protein of IAV, enables binding in a multivalent manner to terminal sialic acid (Sia) residues of surface glycans of the host cell[8]. HA forms a homotrimer with three binding sites for Sia [8-10]. The affinity of binding to monomeric Sia such as α–methylsialic acid and sialyllactose is only in the millimolar range (2-6 mM)[11]. However, the abundantly sialylated surface of host cells enable strong multivalent attachment of IAV with its densely packed HA trimers[12].

One approach to inhibit IAV infections is the development of constructs, which display multiple ligands including sialic acids, aptamers or peptides derived from neutralizing antibodies. All these constructs have in common that they are designed to simultaneously bind to Sia binding sites of several HAs[13]. Indeed, on surfaces with variable receptor concentration, multivalent nanoparticles and polymers have been shown to selectively enhance binding[14, 15]. Polymers[16, 17], liposomes[18] and proteins[19] have been utilized as scaffolds for such multivalent IAV inhibitors, yet their use as templates for structurally defined inhibitors binding HA is often limited by an inherent polydispersity and backbone flexibility. To date, only few examples of binders with a geometric arrangement that matches that of HA binding sites have been described. Such scaffolds have been constructed either through the use of a defined arrangement of ligands[20, 21] or the integration of a peptide sequence from neutralizing HA antibodies into the computational design of a high-affinity trimeric HA binder[22]. These examples illustrate that there is a need, in the case of rigid templates, for an optimal placement of ligands in a structurally reproducible three-dimensional orientation to achieve binding of HA[23, 24]. Yet, challenges remain in the rational design of potent IAV inhibitors at useful quantities, especially given the heterogeneity of IAV strains responsible for seasonal influenza outbreaks[25]. Ideally, the highly conserved HA-Sia binding site of different IAV subtypes could be targeted by the same protein scaffold to produce inhibitors with broader antiviral activity.

Here, we propose a new approach for influenza targeting based on bacteriophage capsids as rigid protein scaffolds which provide a structurally defined presentation of sialic acid ligands to match the binding sites of the trimeric HA. We reasoned that such a structure-guided arrangement should also result in efficient binding of viruses and ultimately prevent virus interaction with and infection of host cells. Bacteriophage capsids are increasingly used in cell targeting[26] and drug delivery[27]. Recent studies have taken advantage of the capsids' monodispersity and the ease of incorporation of bioorthogonal amino acids to achieve site-

specific conjugation of a defined number of ligands[26]. We go one step further and exploit the compact symmetrical 3D capsid structure itself as a means of targeting the trimeric HA ectodomain, which also opens up the possibility of rationalizing experimental data through statistical mechanics modeling of capsid-HA interactions.

We identified icosahedral bacteriophages Qβ as the most suitable candidates among phages for a display of Sia. The Qβ capsid has a diameter of around 25 nm and consists of 180 copies of a 14.1 kDa coat protein[28, 29]. The symmetric structure of the capsid permits the use of amino acid residue at position 16 in the Qβ coat protein sequence for triangular geometries with distances of 5-6 nm. This structural aspect provides an ideal system for the anchoring of sialic acid ligands with different linker lengths to match the distance between their individual binding sites (~ 4.7 nm) on the HA trimer (**Fig. 1a**). We have previously shown that Sia binding affinity to HA is very sensitive to exact spacing[20].

Escherichia coli is the preferred expression system to produce Qβ bacteriophage capsids and to allow subsequent chemical functionalization[26, 30]. Specifically, based on a report in which recombinant protein expression was achieved with L-homopropargylglycine (Hpg)[26, 30] in Qβ-mutant at position 16 (Qβ(K16Hpg) = Qβ[Hpg]), we conjugated ethylene glycol (EG)-linked sialosides to the phage capsids through copper-catalyzed azide-alkyne cycloaddition (CuAAC) (**Fig. 1b**). To identify the length of the linker that is optimal for binding, we conjugated sialic acid azides with mono-, -tri, -penta or octaethylene glycol linkers (Sia1, Sia3, Sia5 and Sia8) that were synthesized according to established[31]. In addition, we linked *N*-acetylgalactosamine with a triethylene glycol linker (Gal3) to develop negative control binders as well as α-2,6- and α-2,3-sialyllactose (2.6SL and 2.3SL) to probe the Qβ-conjugates for distinction of human and avian influenza viruses. ESI-MS analysis of the intact protein verified the full conversion of the alkyne-containing Qβ-capsids to the corresponding sialic acid-glycoconjugates. Tryptic in-gel digestion followed by LC-MS/MS analysis of the Qβ[Sia] and Qβ[Gal3] constructs confirmed that position 16 in the coat protein sequence had been successfully modified by the respective sugars. It is important to note that using the sialoside carrying an azide moiety directly at the anomeric C-2 carbon ('Sia0') led to incomplete conversion of Qβ[Hpg].

We first characterized the affinity at which these constructs bind to the A/X31 virus, which is of the H3N2 subtype. Microscale thermophoresis (MST) measurements revealed apparent dissociation constants ($K_{D,app}$) in the lower nanomolar range of capsid particles (**Fig. 1c**, **Table 1**). Extending the linker length weakens binding, as indicated by an increase of $K_{D,app}$. This clearly points towards Qβ[Sia1], carrying the shortest linker in the series, as the most potent binder. As expected, Qβ[Gal3] did not exhibit any interaction with A/X31.

Hemagglutination inhibition (HAI) assays confirmed our MST findings, again revealing that Qβ[Sia1] was the best binder with an HAI constant (K_iHAI) of 1.3±0.5 nM (**Fig. 1c**, **Table 1**). This value corresponds to an enhancement in sialic acid binding by a factor of ~10^5 (based on the actual sialic acid concentration of K_iHAI x 180 (coat protein monomers). To the best of our knowledge, an enhancement in binding of this strength is rather unique for sialic acid moieties presented in a defined multivalent fashion.

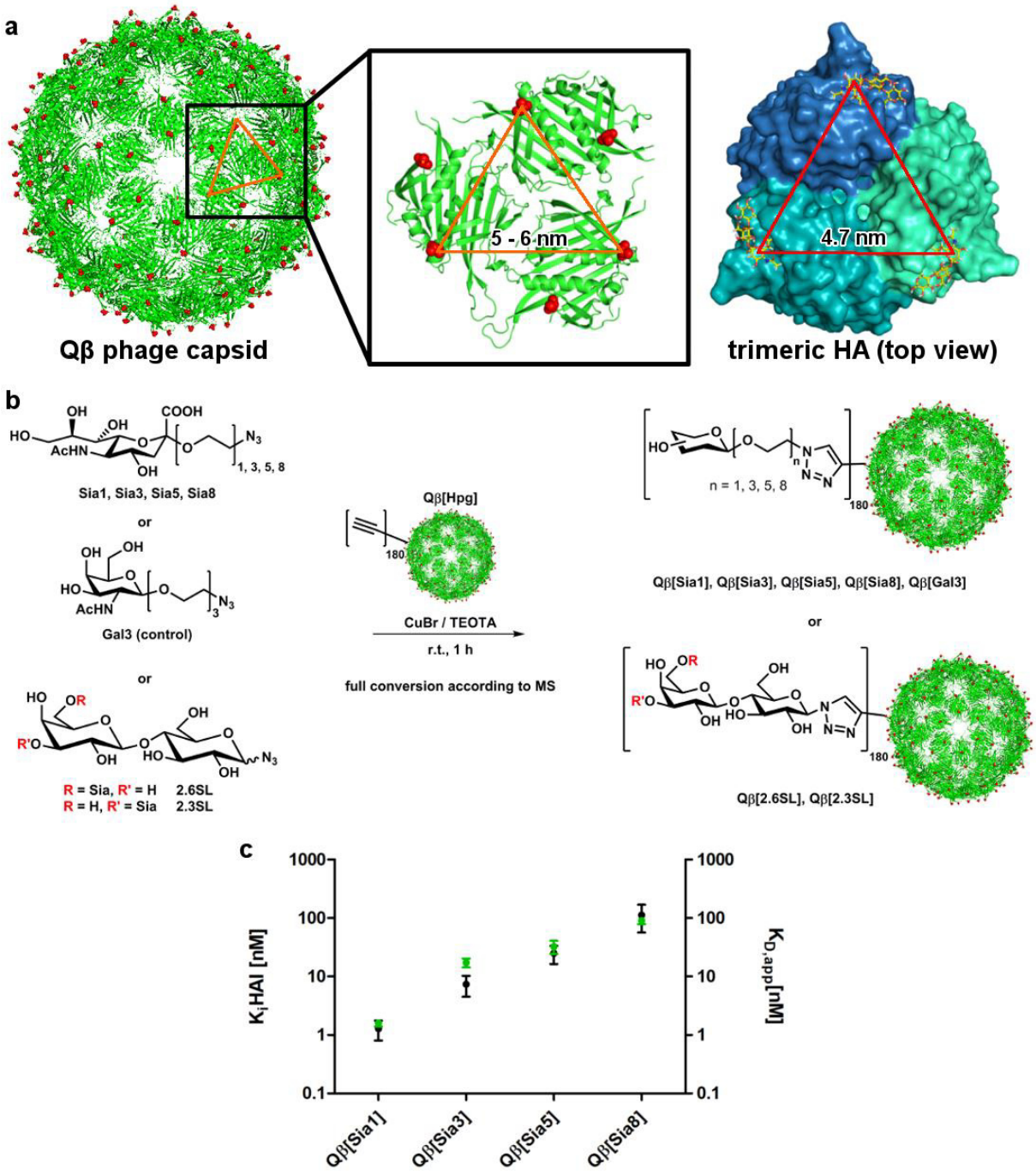

Fig. 1. **Functionalized Qβ phage capsids as high affinity IAV binders.** (**a**) Structural match between distances of HA-Sia binding pockets (pdb: 1HGG; A/X31) and distances of sialic acid attachment points (position K16 of wild type Qβ coat protein – red dots) on the capsid surface (pdb 1QBE). (**b**) Recombinantly expressed Qβ[Hpg] was conjugated with sialic acid azides by means of CuAAC (see Supplementary Information). (**c**) HAI assays against 4 HAU A/X31: K_iHAI (black); and $K_{D,app}$ (green) measured by microscale thermophoresis (MST). Error bars for K_iHAI indicate the SEM (N≥4), and for $K_{D,app}$ the SEM (N≥3).

Analysis of Qβ[Sia] binding using cryogenic transmission electron microscopy (cryo-TEM) revealed that A/X31 virions were densely decorated by Qβ[Sia1] capsid particles (**Fig. 2b,c**). Extension of linker length reduced binding, as illustrated for Qβ[Sia5] (**Supplementary Figure**

1). As expected, Qβ[Hpg] (**Supplementary Figure 1**) and Qβ[Gal3] (**Fig. 2a**) failed to interact with the H3N2 IAV.

We used cryo-electron tomography (cryo-ET) to obtain unequivocal information on local 3D structure. Reconstructions of tomography series (±65° at 2° angular increment) clearly showed that very high quantities of Qβ[Sia1] capsids were directly bound to HA spikes in the viral envelope. A systematic evaluation strongly suggested that single capsids typically interact with only one individual, trimeric HA spike protein (**Fig. 2d-f**).

To determine whether individual HA trimers can bind to capsids, we incubated capsids with HA ectodomains obtained through bromelain treatment of intact viruses. The experiment revealed that HA ectodomains bind in a mostly perpendicular orientation to Qβ[Sia1] capsids (**Fig. 2g**). Given the low affinity of monomeric binding to Sia, our observations strongly suggest that binding to an HA trimer engages more than one valency of the sialylated capsid surface.

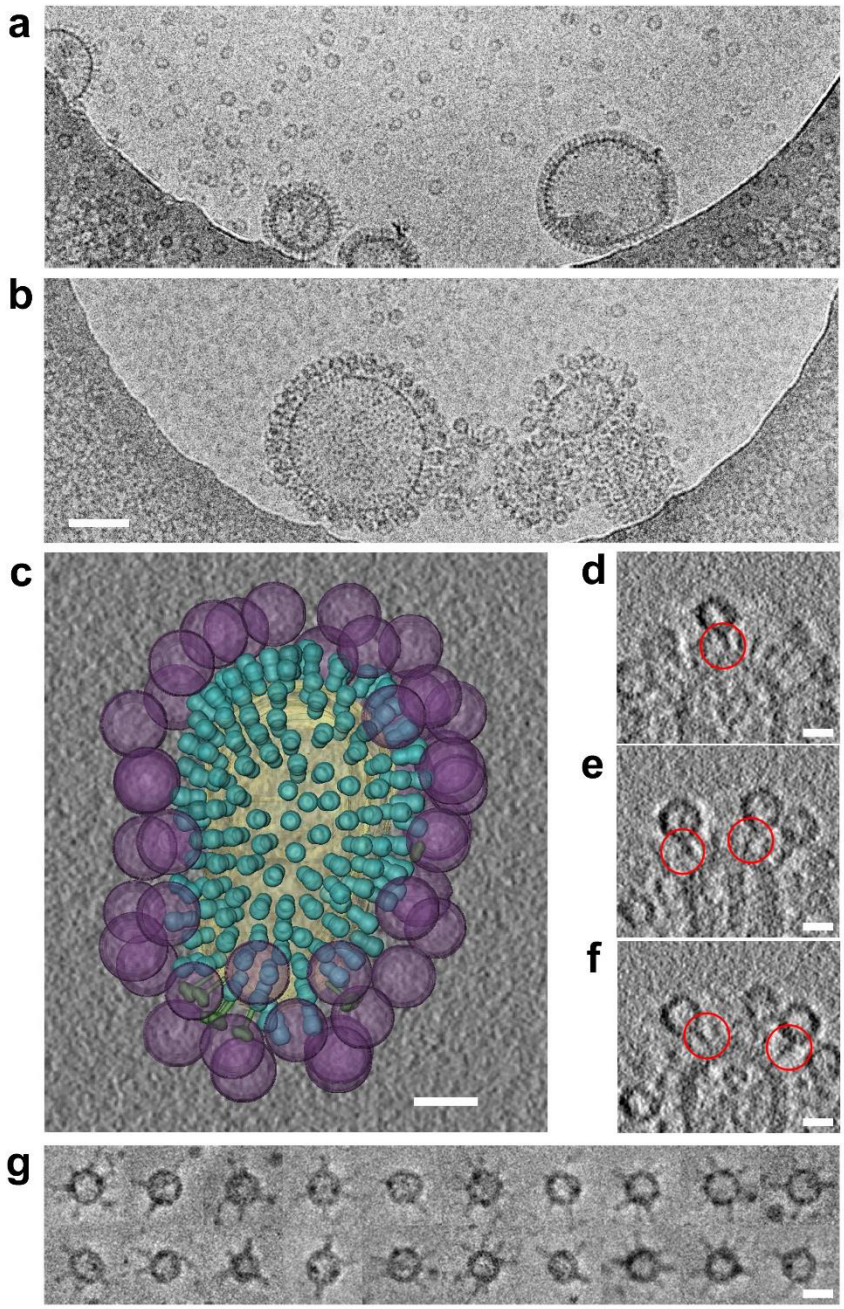

Fig. 2. **Cryo-TEM images of A/X31 incubated with diverse Qβ phage capsids**. (**a**) Qβ[Gal3], (**b**) Qβ[Sia1] (Scale bar: 100 nm). (**c**) Model of HA and neuraminidase (NA) distribution and the spatial arrangement of 42 Qβ[Sia1] capsids bound to an individual virion on basis of the 3D structure reconstructed from cryo-ET data. Color code: Virus envelope (yellow), HA (cyan), NA (green), phage capsids (purple). The limited resolution does not permit a clear definition of the rotational orientation of the HA monomers. Therefore, rotational averaged models for HA trimers were fitted in the corresponding densities (scale bar: 25 nm). (**d-f**) Selected sections (0.54 nm) of tomograms indicating individual binding events (red circles) of Qβ[Sia1] to HA trimer (scale bars: 20 nm). (**g**) A gallery of 20 selected subimages indicating binding of bromelain-cleaved HA ectodomains of influenza A/X31 virus to individual Qβ[Sia1] (scale bar: 20 nm).

Our experimental results indicate that the remarkably low values of $K_{D,app}$ are based on the interaction of single HA trimers with a maximum of three Sia residues each. To test and rationalize this conclusion by an independent and complementary approach, we applied statistical mechanics modeling.

On the Qβ capsid surface neighboring Sia units form triplets (**Fig 3a**) whose geometry is similar to that of the HA trimer. The comparison of the binding energy per capsid and the deformation energy of the virus (c.f. **Supplementary Notes**) revealed that capsid binding is not strong enough to bend the virus surface, suggesting that each Qβ capsid binds to only one HA spike, which matches our cryo-TEM results (**Fig. 2g**). Analyzing mono-, di-, and trivalently bound capsids (**Supplementary Figure 2j**), we find that the dissociation constant is dominated by trivalent binding. Even for the longest EG-linkers, where the relative contribution of mono and divalent binding is most pronounced, approximating the dissociation constant solely by trivalent binding alters the result by less than 15%. The dissociation constant, in terms of capsid concentration, of the Sia triplets towards HA reads (see **Supplementary Notes**):

$$K_D = \frac{K_{mono}^3 \omega_{sia}^3}{60(C_3(d_1)+C_3(d_2))} \qquad \textbf{(Eq. 1)}$$

where each bound Sia unit contributes to K_D with K_{mono}=2.5mM[12], the dissociation constant of monovalent Sia. The factor 1/60 reflects the presence of 60 Sia triplets with an edge length of d_1=5.0 nm and 60 Sia triplets with an edge length of d_2=5.9 nm on the capsid surface (inset in **Fig. 1a**). This enhances the binding affinity by providing a large number of binding states [32]. The dissociation constant depends on the angular restriction factor ω_{Sia} and on the edge-length dependent cooperativity factor C_3 (see below).

ω_{Sia} accounts for the restriction imposed on the rotational degrees of freedom of each Sia unit due to steric repulsion between the Sia unit and the EG linker (c.f. **Supplementary Notes**). From a fit of **Eq.1** to the experimentally measured apparent dissociation constant $K_{D,app}$ (**Fig. 3c**) we find a small value of ω_{Sia}=0.05, which significantly enhances the binding affinity. We note that a variation of ω_{Sia} leads to a shift of the theoretical curve in **Fig. 3c** by a constant value, whereas the position of the minimum is independent of ω_{Sia}.

The cooperativity factor $C_3(d)$ describes the conditional probability that all three Sia units simultaneously bind to an HA binding site in case one Sia unit is already bound. We evaluate C_3, which is given in units of concentration squared, through a numerical integration over all capsid positions and orientations weighted with the stretching probability P_{str} of each linker, taking into account the fact that the capsid cannot penetrate the HA trimer (c.f. **Supplementary Notes**).

To quantify the EG linker stretching probability P_{str} of the EG linkers entering C_3, we performed molecular dynamic (MD) simulations of EG oligomers (CH_3-O-[CH_2-CH_2-O-]$_n$-

CH_3, with n∈[1,10]) in explicit water, and determined the probability $P_{str}(r_{ete})$ that EG extends to an end-to-end distance r_{ete}. In **Fig. 3b** examples for P_{str} are shown for n=1, 3, 5, 8, i.e. for the linker lengths that were used in the experiments.
Based on **Eq.1** and using ω_{Sia}=0.05, the predicted dissociation constant K_D depends on the number of EG linker units, in good agreement with the experimental data (**Fig. 3c**).

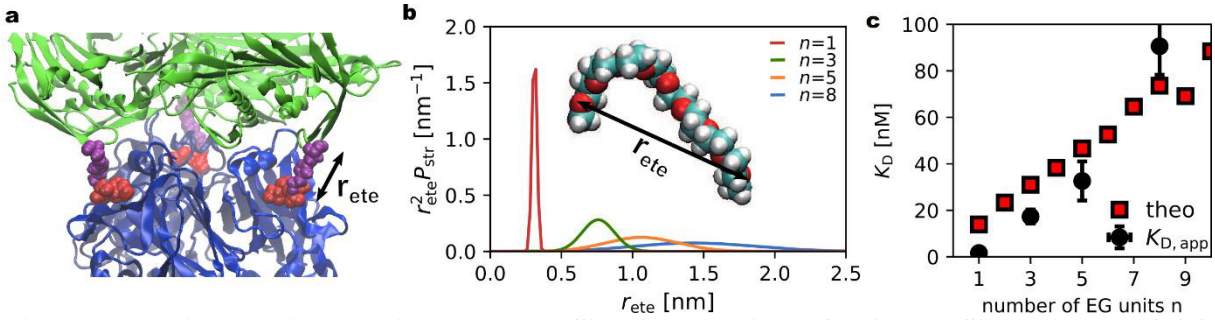

Fig. 3. **Modeling the interaction between Sia binding sites of HA and Sia residues of Qß capsid**. (**a**) Side view of a Qβ capsid (green) bound to HA (blue) in a trimeric binding mode. The Sia units (red) are attached to the Qβ capsid via EG linkers (purple), the end-to-end distance of the linker is denoted by r_{ete}. The conformation is obtained from an energy minimization in vacuum (c.f. **Supplementary Notes**). (**b**) Probability distribution P_{str} of the end-to-end distance multiplied by r^2_{ete} plotted vs. r_{ete}, the distance between the outermost EG oxygen atoms. A snapshot of an EG-oligomer ($n = 8$) is shown in the inset. (**c**) Comparison between the experimental apparent dissociation constant $K_{D,app}$ (grey dots, **Table 1**). and the theoretical dissociation constant K_D (red squares, **Eq.1**) for different EG monomer numbers.

Interestingly, the EG linked Qβ[Sia] capsids were capable of competitively preventing hemagglutination of erythrocytes by several human IAV strains in a fashion that depended on the length of the attached linker (**Table 2**). For one avian IAV and one human influenza B virus strain, however, no inhibition was observed. To test whether human and avian influenza virus strains could be discriminated using more complex sialic acid ligands, we generated Qβ capsids using either the human Qβ[2.6SL] or the avian Qβ[2.3SL] sialic acid ligand analogue. We observed specific binding only between Qβ[2.6SL] and human IAV strains (A/X31 (H3N2), A/WSN/1933 (H1N1)) and of Qβ[2.3SL] to an avian virus (A/teal/Germany/2005 (H5N1)). In contrast, Qβ[2.6SL] capsids did not yield in measurable K_iHAI values using an avian IAV. Similarly, Qβ[2.3SL] capsids did not yield K_iHAI values using human IAV strains (

Table 3). Additionally, the Qβ[2.6SL] capsids were able to efficiently inhibit hemagglutination of a human influenza B virus (B/Thüringen/2/2006) (K_iHAI = 1.7±1.1 nM).

While Qβ[Sia1] was most efficient in binding to HA of A/X31 as confirmed by statistical mechanics modeling, we found experimentally that Qβ[Sia3] and Qβ[Sia5] capsids exhibited most efficient binding to H1 (HA from H1N1 viruses; **Table 2**). The reason could be differences in the globular head arrangement (c.f. **Supplementary Notes**) and/or the glycosylation pattern[33] of the HA ectodomain. This correlates to our previous work using display of sialic acid moieties on rigid DNA-PNA scaffolds in which we showed that binding affinity to HA is very sensitive to matching the distance between binding units and the distance between neighboring binding pockets[20].

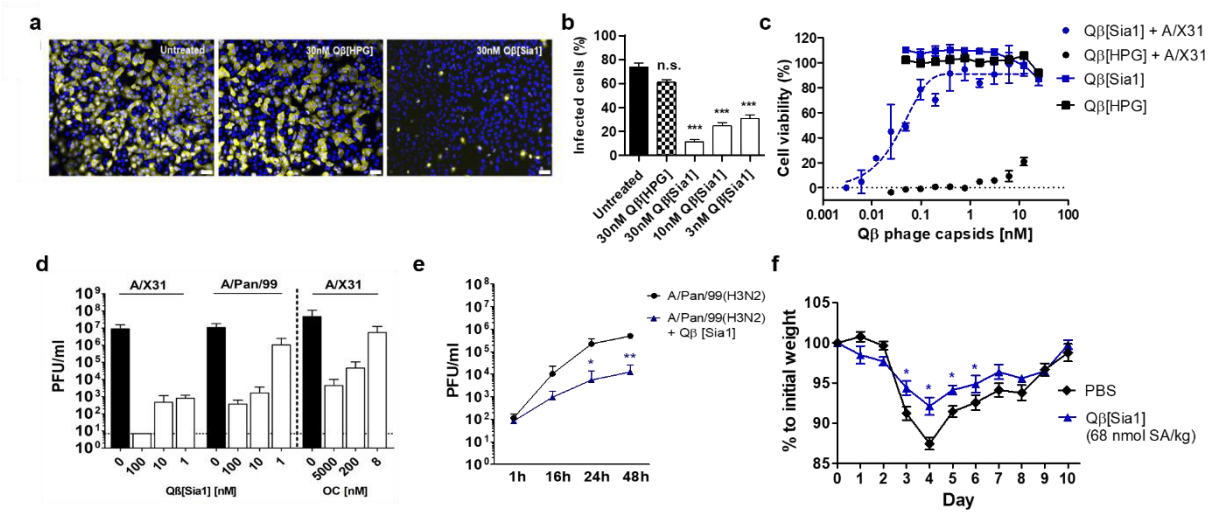

Fig. 4. **Inhibitory potential of Qβ[Sia1] against various IAV strains.** (**a**) Inhibition of influenza A/Panama/2007/1999 virus (Pan/99) infection of A549 cells by Qβ[Sia1] capsids. Infected cells were identified through confocal imaging (A, bar = 40 µm) of the viral NP protein (yellow) nuclei (blue as revealed by DAPI staining). (**b**) Representation of the percentage of A/Pan/99 infected cells based on the NP signal from fluorescence images (see **a**). Infection inhibition with different concentrations of Qβ[Sia1] was determined relative to an untreated control. (**c**) Infection inhibition of A/X31 by Qβ[Sia1] or Qβ[Hpg] (as a control) and cell toxicity caused by Qβ[Sia1] or Qβ[Hpg] (absence of A/X31) as determined by a cell viability test. Error bars in **b** and **c** indicate SEM (N=3). (**d**) Influenza virus titers from supernatants of MDCK-II cells infected (MOI 0.01) for 24 hrs in the presence or absence of Qβ[Sia1] or Oseltavimir carboxylate (OC) at the indicated concentrations. Columns represent the mean of three independent experiments in duplicates and error bars indicate SD. (**e**) *Ex vivo* human lung tissue infection inhibition using 10 nM Qβ[Sia1] against A/Pan/99. Error bars indicate SD (N=4). (**f**) Protective potential of Qβ[Sia1] capsids against A/X31 infections in Balb/c mice. The error bars show SEM (N=10). (**b**), (**d**) were statistically analyzed using a One-Way ANOVA, and (**f**) using a two-tailed Mann-Whitney test (*=p<0.05, **=p<0.001, ***=p<0.0001).

To determine the extent to which Qβ[Sia1] might prevent infections, we infected several host systems with A/X31 or seasonal A/Panama/2007/1999 virus (A/Pan/99) in the presence of inhibitors. Upon preincubation, we observed an effective inhibition of infections of human alveolar epithelial A549 cells, as revealed by quantification of the viral nucleoprotein (NP) detected inside cells (**Fig. 4a,b**). An IC_{50} value of 0.04 nM for Qβ[Sia1] capsids was measured in a cell viability assay (**Fig. 4c**) using A/X31. Strikingly, the inhibitory potential was much higher than suggested by results from the binding inhibition experiments. We hypothesize that this is due to the presence of the inhibitor in solution throughout the entire multi-step infection experiment. To assess the efficacy of these phage capsids in reducing multicyclic virus replication we infected MDCK-II cells at low multiplicity with A/X31 and A/Pan/99, respectively, and incubated them for 24 hrs in the presence of increasing Qβ[Sia1] concentrations (**Fig. 4d**). Plaque titrations showed a strong reduction of virus growth up to six log-scales when cells were treated with 100 nM Qβ[Sia1] (**Fig. 4d**). In comparison, the inhibitory effect of Oseltamivir carboxylate, a well-established inhibitor of IAV neuraminidase, was weaker despite higher concentrations applied (**Fig. 4d**). Mimicking more native conditions for human lungs, we showed that Qβ[Sia1] significantly reduced virus titers in the supernatants of human lung tissue infected *ex vivo*. In this therapeutic setup, treatments with Qβ[Sia1] were administered only after infection (**Fig. 4e**). To probe for an innate immune response caused by

Qβ phage capsids, which could harm the host by inducing severe inflammation, we analyzed cytokine release from lung tissue after incubation with phage capsids. In order to rule out any side effects due to residual contamination toxin traces, which might cause inflammatory response, in particular by LPS originating from E. coli, we compared cytokine release levels from lung tissue to an LPS standard. In fact, Qβ capsids did not induce significant levels of TNF-α, IL-1ß or IFN-β, regardless whether they were purified by the standard protocol being already efficient in clearance of LPS or subjected to an additional LPS removal procedure **(Fig. 4e**, **Supplementary Figure 3**). For both purification protocols, similar virus titer reductions were obtained (**Supplementary Figure 4**). Notably, we found that levels of IFN-β as signature antiviral cytokine were significantly reduced after treatment of infected tissue with Qβ capsids. This result strongly suggests that the antiviral activity of phage capsids is conferred by their binding to viruses and not mediated by antiviral cytokine induction or a proinflammatory cell response.

In order to corroborate the antiviral effects of our construct *in vivo*, we showed that the loss of body weight in mice after infection with A/X31 was significantly reduced upon pretreatment with Qβ[Sia1] capsids indicating lower morbidity (**Fig. 4f**). We are not aware that phage capsids have been examined so far for stimulation of innate responses in explanted human lung tissue. The observed poor cytokine induction in the lung cultures is in line with a study on applying phage therapy for acute pneumonia of BALB/c mice caused by multi-drug-resistant *Pseudomonas aeruginosa* [34], showing that pseudomonal phage PAK_P1 did not cause a significant increase in cytokine production and was immunologically well tolerated.

In conclusion, our study demonstrates that structurally defined, functionalized Qβ capsids can serve as modular and adaptable platforms to generate multivalent ligands for influenza virus targeting. We suggest our findings demonstrate that these ligands function as highly efficient and specific IAV inhibitors and have large potential to be developed into novel antivirals for the treatment of influenza.

Acknowledgements

We would like to thank Andrew K. Udit for providing the Qβ(K16M) plasmid. This work was supported by the German Research Foundation (DFG, SFB765 and TR84) and the Germany Ministry of Education and Research (BMBF, RAPID) as well as Charité 3R.

Author Contributions

D.L., S.K., S.L., K.L., M.W., L.E.S., A.Ha., N.B., R.R.N., K.O., A.C.H., S.H., T.W., A.H., and C.P.R.H. designed the study. D.L., S.K, S.N., S.B., M.S., S.S., S.F., K.H., U.H., M.B., L.A., L.Y., performed the experiments. S.N. performed the capsid expression. K.L., S.D.C., and C.B. performed electron microscopy and image analyses. J.N. carried out surgical interventions and prepared lung excisions. S.L. performed modelling, simulations, and calculations. D.L., S.K., S.L., A.H., T.W. and C.P.R.H. prepared the manuscript. All authors discussed the results and reviewed the manuscript.

Competing Interests

The authors declare no competing interests.

Table 1: $K_i HAI$ values and $K_{D,app}$ measured by MST against A/X31. SEM (N≥3) is given in parenthesis.

	K_iHAI (nM)	$K_{D,app}$ (nM)
Qβ[Sia1]	1.3 (±0.5)	1.6 (±0.2)

Qβ[Sia3]	7.4 (±2.9)	17.3 (±3)
Qβ[Sia5]	25.0 (±8.5)	32.6 (±8.4)
Qβ[Sia8]	112.5 (±56.1)	90.6 (±12.3)
Qβ[Gal3]	>500	>500
Qβ[Hpg]	>500	n.d.

Table 2: Strain specific binding to different IAV strains depending on the attached linker length represented by the corresponding $K_i HAI$ values. SEM (N≥3) is given in parenthesis.

Virus strain	Qβ[Sia1]	Qβ[Sia3]	Qβ[Sia5]	Qβ[Sia8]	Qβ[Gal]	Qβ[HPG]
A/X31 (H3N2)	1.3 (±0.5)	7.4 (±2.9)	25.0 (±8.5)	112.5 (±56.1)	>500	>500
A/Panama/2007/1999 (H3N2)	3.1 (±0.6)	>100	>100	>100	>100	>100
A/mallard/Germany/439/2004 (H2N3)	25.0 (±4.2)	>100	>100	>100	>100	>100
A/Puerto Rico/8/1934 (H1N1)	>100	25.0 (±0.0)	25.0 (±0.0)	50.0 (±16.7)	>100	>100
A/WSN/1933 (H1N1)	>100	12.5 (±4.2)	12.5 (±0)	12.5 (±0)	>100	>100
A/teal/Germany/2005 (H5N1)	>100	>100	>100	>100	>100	>100
B/Thüringen/2/2006	>100	>100	>100	>100	>100	>100

Table 3: Specific binding of Qβ[2.6SL] and Qβ[2.3SL] to relevant human (A/ X31 and A/WSN/1933) and avian (A/teal/Germany/2005) influenza virus strains, respectively. SEM (N≥3) is given in parenthesis.

Virus strain	Qβ[2.6SL]	Qβ[2.3SL]
A/X31 (H3N2)	41.7 (±10.4)	>250
A/WSN/1933 (H1N1)	52.1 (±10.4)	>250
A/teal/Germany/2005 (H5N1)	>250	9.1 (±3.4)
B/Thüringen/2/2006	1.7 (±1.1)	>250

References

1. Fasting, C. et al. Multivalency as a chemical organization and action principle. *Angew. Chem. Int. Ed.* **51,** 10472–10498 (2012).
2. Gestwicki, J.E., Cairo, C.W., Strong, L.E., Oetjen, K.A. & Kiessling, L.L. Influencing receptor−ligand binding mechanisms with multivalent ligand architecture. *J. Am. Chem. Soc.* **124,** 14922–14933 (2002).
3. Kiessling, L.L., Gestwicki, J.E. & Strong, L.E. Synthetic multivalent ligands in the exploration of cell-surface interactions. *Curr. Opin. Chem. Biol.* **4,** 696–703 (2000).
4. Branson T.R. et al. A protein-based pentavalent inhibitor of the cholera toxin B-subunit. *Angew. Chem. Int. Ed.* **53**, 8323-8327 (2014).
5. Wu, N.C. & Wilson, I.A. Structural insights into the design of novel anti-influenza therapies. *Nat. Struct. Mol. Biol.* **25,** 115-121 (2018).
6. Kadam, R.U. et al. Potent peptidic fusion inhibitors of influenza virus. *Science* (2017).

7. van de Wakker, S.I., Fischer, M.J.E. & Oosting, R.S. New drug-strategies to tackle viral-host interactions for the treatment of influenza virus infections. *Eur. J. Pharmacol.* **809,** 178-190 (2017).
8. Weis, W. et al. Structure of the influenza virus haemagglutinin complexed with its receptor, sialic acid. *Nature* **333,** 426–431 (1988).
9. Sauter, N.K. et al. Crystallographic detection of a second ligand binding site in influenza virus hemagglutinin. *Proc. Natl. Acad. Sci. U. S. A.* **89,** 324–328 (1992).
10. Stevens, J. et al. Structure of the uncleaved human H1 hemagglutinin from the extinct 1918 influenza virus. *Science* **303,** 1866–1870 (2004).
11. Sauter, N.K. et al. Hemagglutinins from two influenza virus variants bind to sialic acid derivatives with millimolar dissociation constants: A 500-MHz proton nuclear magnetic resonance study. *Biochemistry* **28,** 8388–8396 (1989).
12. Mammen, M., Choi, S.-K. & Whitesides, G.M. Polyvalent interactions in biological systems: implications for design and use of multivalent ligands and inhibitors. *Angew. Chem. Int. Ed.* **37,** 2754–2794 (1998).
13. Lauster, D. et al. Multivalent peptide–nanoparticle conjugates for influenza-virus inhibition. *Angew. Chem. Int. Ed.* **56,** 5931-5936 (2017).
14. Curk, T., Dobnikar, J. & Frenkel, D. Optimal multivalent targeting of membranes with many distinct receptors. *Proc. Natl. Acad. Sci. U. S. A.* **114,** 7210-7215 (2017).
15. Martinez-Veracoechea, F.J. & Frenkel, D. Designing super selectivity in multivalent nano-particle binding. *Proc. Natl. Acad. Sci. U. S. A.* **108,** 10963-10968 (2011).
16. Mammen, M., Dahmann, G. & Whitesides, G.M. Effective inhibitors of hemagglutination by influenza virus synthesized from polymers having active ester groups. Insight into mechanism of inhibition. *J. Med. Chem.* **38,** 4179–4190 (1995).
17. Kwon, S.-J. et al. Nanostructured glycan architecture is important in the inhibition of influenza A virus infection. *Nat. Nanotech.* **12,** 48-54 (2017).
18. Kingery-Wood, J.E., Williams, K.W., Sigal, G.B. & Whitesides, G.M. The agglutination of erythrocytes by influenza virus is strongly inhibited by liposomes incorporating an analog of sialyl gangliosides. *J. Am. Chem. Soc.* **114,** 7303–7305 (1992).
19. Wang, H. et al. Design and synthesis of glycoprotein-based multivalent glyco-ligands for influenza hemagglutinin and human galectin-3. *Bioorg. Med. Chem.* **21,** 2037–2044 (2013).
20. Bandlow, V. et al. Spatial screening of hemagglutinin on influenza A virus particles: sialyl-LacNAc displays on DNA and PEG scaffolds reveal the requirements for bivalency enhanced interactions with weak monovalent binders. *J. Am. Chem. Soc.* **139,** 16389-16397 (2017).
21. Waldmann, M. et al. A nanomolar multivalent ligand as entry inhibitor of the hemagglutinin of avian influenza. *J. Am. Chem. Soc.* **136,** 783-788 (2014).
22. Strauch, E.-M. et al. Computational design of trimeric influenza-neutralizing proteins targeting the hemagglutinin receptor binding site. *Nat. Biotechnol.* **35,** 667 (2017).
23. Vonnemann, J. et al. Size dependence of steric shielding and multivalency effects for globular binding inhibitors. *J. Am. Chem. Soc.* **137,** 2572–2579 (2015).
24. Liese, S. & Netz, R.R. Quantitative prediction of multivalent ligand–receptor binding affinities for influenza, cholera, and anthrax inhibition. *ACS Nano* **12,** 4140-4147 (2018).
25. Yang, H. et al. Structure and receptor binding preferences of recombinant human A(H3N2) virus hemagglutinins. *Virology* **477,** 18-31 (2015).
26. Ribeiro-Viana, R. et al. Virus-like glycodendrinanoparticles displaying quasi-equivalent nested polyvalency upon glycoprotein platforms potently block viral infection. *Nat Commun.* **3,** 1303 (2012).

27. Wu, W., Hsiao, S.C., Carrico, Z.M. & Francis, M.B. Genome-free viral capsids as multivalent carriers for taxol delivery. *Angew. Chem. Int. Ed.* **48,** 9493–9497 (2009).
28. Valegård, K., Fridborg, K. & Liljas, L. Crystallization and preliminary X-ray diffraction studies of the bacteriophage Qbeta. *Acta Crystallogr., Sect. D: Biol. Crystallogr.* **50,** 105–109 (1994).
29. Golmohammadi, R., Fridborg, K., Bundule, M., Valegård, K. & Liljas, L. The crystal structure of bacteriophage Q beta at 3.5 A resolution. *Structure* **4,** 543–554 (1996).
30. Strable, E. et al. Unnatural amino acid incorporation into virus-like particles. *Bioconjugate Chem.* **19,** 866–875 (2008).
31. Crich, D. & Li, W. α-Selective sialylations at −78 °C in nitrile solvents with a 1-adamantanyl thiosialoside. *J. Org. Chem.* **72,** 7794–7797 (2007).
32. Hunter, C.A. & Anderson, H.L. What is cooperativity? *Angew. Chem. Int. Ed.* **48,** 7488-7499 (2009).
33. Tate, M. et al. Playing hide and seek: how glycosylation of the influenza virus hemagglutinin can modulate the immune response to infection. *Viruses* **6,** 1294-1316 (2014).
34. Roach et al. Synergy between the host immune system and bacteriophage is essential for successful phage therapy against an acute respiratory pathogen, *Cell Host & Microbe* **22**, 38-47 (2017)

Code Availability
Custom code is available from the corresponding author (S.L.).

Data Availability
The data that support the findings of this study are available within the paper and its Supplementary Information.